On-chip electrically controlled routing of photons from a single quantum dot

C. Bentham,[1] I. E. Itskevich,[2,a)] R. J. Coles,[1] B. Royall,[1] E. Clarke,[3] J. O'Hara,[1] N. Prtljaga,[1] A. M. Fox,[1] M. S. Skolnick,[1] and L. R. Wilson[1]
[1]*Department of Physics and Astronomy, University of Sheffield, Sheffield S3 7RH, United Kingdom*
[2]*School of Engineering, University of Hull, Hull HU6 7RX, United Kingdom*
[3]*Department of Electronic and Electrical Engineering, University of Sheffield, Sheffield S1 3JD, United Kingdom*

(Received 31 March 2015; accepted 20 May 2015; published online 1 June 2015)

Electrical control of on-chip routing of photons emitted by a single InAs/GaAs self-assembled quantum dot (SAQD) is demonstrated in a photonic crystal cavity-waveguide system. The SAQD is located inside an H1 cavity, which is coupled to two photonic crystal waveguides. The SAQD emission wavelength is electrically tunable by the quantum-confined Stark effect. When the SAQD emission is brought into resonance with one of two H1 cavity modes, it is preferentially routed to the waveguide to which that mode is selectively coupled. This proof of concept provides the basis for scalable, low-power, high-speed operation of single-photon routers for use in integrated quantum photonic circuits.
[http://dx.doi.org/10.1063/1.4922041]

Semiconductor photonic quantum information technology is progressing rapidly as nanoscale photonic circuits are being developed, in which single photon states are generated, manipulated, and detected.[1,2] Provision of controllable single-photon sources and the distribution of their emission into the circuit are crucial for this development. Individual self-assembled quantum dots (SAQDs), with discrete energy spectra due to zero-dimensional confinement, provide an attractive option[3,4] because of mature fabrication technology, the relative ease of incorporation in advanced semiconductor nanostructures and on-demand emission. Individual SAQDs can deliver both an efficient on-chip source of antibunched photons and a natural light-matter interface.

The optical properties of single SAQDs can be dramatically enhanced if they are incorporated within photonic crystal (PhC) cavities, which modify the local optical mode density experienced by the SAQD emitter.[2] This provides considerable opportunities for the development of components of quantum photonic circuits. Cavities with large Q-factor in the strong coupling regime are required for observation of fundamental light-matter interaction phenomena such as photon blockade,[5] which can be exploited for the development of optical transistors[6] and quantum gates.[7] However, advances have also been reported in the weak coupling regime, which is achievable for cavities with a relatively low Q-factor of several thousand. As an example, coupling of non-classical light to low-loss waveguide modes and the subsequent distribution of single photons in a quantum photonic circuit have been successfully demonstrated.[8–10]

Nonetheless, whilst the distribution of quantum light on a semiconductor chip has been reported, control has not yet been demonstrated. The ability to control photon routing at the point of generation would represent an important step-forward in the development of semiconductor-based quantum photonic integrated circuits. A proof-of-concept experimental demonstration of an electrically controllable on-chip optical router using a single SAQD as an emitter is presented in this paper.

Our approach to achieve on-chip photon routing is based on using an H1 cavity in a hexagonal PhC membrane, illustrated in Fig. 1(a) (discussed in detail later).[11] There are two fundamental dipole modes in an H1 cavity, nominally degenerate, but the degeneracy is lifted due to fabrication imperfections. The small mode volume of H1 cavities facilitates efficient coupling of the emission from incorporated SAQDs to the modes. In addition, two line-defect W1 waveguides are incorporated in the PhC, providing two distinct propagation channels. Selective coupling of each of the cavity modes to its respective waveguide is accomplished by waveguide orientation in the crystal. In this case, photons can be directed into one of two propagation channels, dependent on which cavity mode they are coupled to.

In Ref. 11, ensemble photoluminescence (PL) from incorporated SAQDs provided a photon source. For optical quantum information applications however, single-photon emission from individual SAQDs is needed. For efficient coupling, a single-dot emission line should be on resonance with a cavity mode. In order to control the resonance conditions, tunability of either the cavity modes or the SAQD emission (or both) is required (not needed for ensemble PL). Moreover, the tunability should be fast, controllable, easily reversible, and achievable at low power without affecting other parts of the electronic and photonic circuitry. Tuning the SAQD emission by varying the electric field satisfies these criteria, in contrast to other methods suggested so far, such as gas deposition[12] or temperature variation.[13] In the presence of an electric field, the SAQD emission energies change due to the quantum-confined Stark effect (QCSE).[14] The electric field can be varied in a PhC membrane fabricated from a *p-i-n* diode, which constitutes a technological challenge. However, successful development of PhC membranes

a)Author to whom correspondence should be addressed. Electronic mail: I.Itskevich@hull.ac.uk

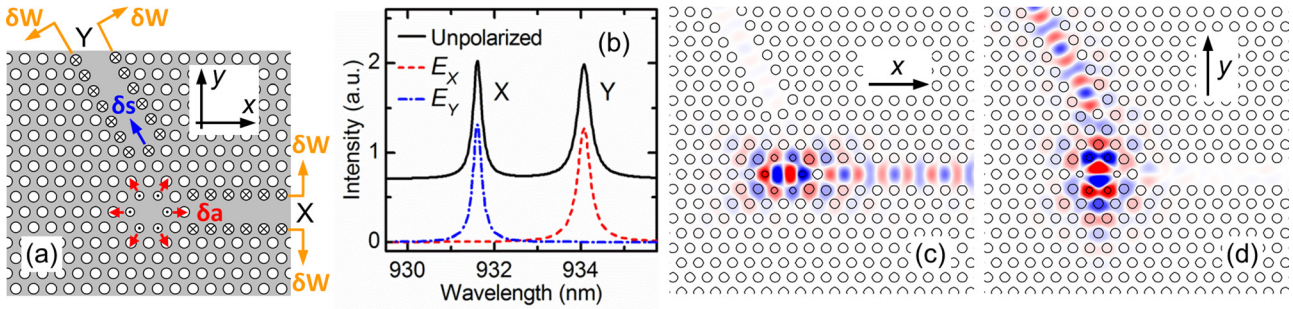

FIG. 1. (a) Schematic diagram of the photonic crystal design, showing the H1 cavity and two W1 waveguides, X and Y. For device optimisation, holes adjacent to the waveguides and to the cavity (denoted by crosses and dots, respectively) are displaced, as indicated by arrows; in addition, the radius of the ring of holes adjacent to the cavity centre is reduced. (b)–(d) Results of modelling for waveguide-coupled non-degenerate cavity modes. (b) Cavity mode spectra for non-polarised, *x*- and *y*-polarised dipole sources (solid black, dashed red, and dashed-dotted blue, respectively). The non-polarised spectrum is offset for clarity. X and Y denote X- and Y-dipole modes, see discussion in the text. (c) Normalised H_z profile for the X-dipole mode. A linear red-white-blue colour scale represents field strength in the range from −92% to 92%, with positive and negative values shown by red and blue, respectively. Magnitudes below −92% and above 92% are shown by saturated colours. (d) The same as (c) for the Y-dipole mode.

with electrically tuneable SAQD emission has been reported.[15]

Here, we demonstrate voltage-controllable routing of emission from a single SAQD in a PhC membrane with an H1 cavity and two W1 waveguides. The membrane is fabricated from a *p-i-n* diode and by changing voltage, the dot emission can be tuned across both cavity modes due to the QCSE. By tuning voltage, we can selectively direct single-dot emitted photons into one of two waveguides, enabling voltage-controllable optical routing. This preferential channeling is observed when, at a specific voltage, the dot emission line is in resonance with the mode coupled to that waveguide. This confirms that the routing is accomplished by resonant coupling of the dot emission to the cavity modes.

Figure 1(a) shows a schematic diagram of the device design. A hexagonal PhC membrane incorporates an H1 cavity and two W1 waveguides, denoted by X and Y, at 120° to one another. The design was optimised by means of finite-difference time-domain (FDTD) computational modeling (details are available in Ref. 11) using MEEP, a freely available software package.[16] The relationship between the PhC slab height, $h = 200$ nm, and the period, a, was selected as $h = 0.85a$ (i.e., $a = 236$ nm); the hole radius, r, varied between $0.31a$ and $0.34a$ (i.e., between 73 nm and 80 nm). This ensured that the fundamental cavity modes spectrally coincide with the SAQD ground-state ensemble emission. To maximise the cavity Q-factor, the ring of holes adjacent to the cavity centre was displaced by $\delta a = 0.091a$ away from the cavity [shown by arrows in Fig. 1(a)] with reduced hole radii $\delta r = 0.091a$.[17] The separation between the cavity and the waveguides was chosen to provide efficient selective coupling without significantly compromising the cavity Q-factor. The waveguides were designed such that each of them sustains a single propagating TE-like mode in the spectral range of the SAQD emission. The first rows of holes in each waveguide were displaced laterally by $\delta W = 0.08a$ so that the cavity modes do not coincide with the cut-off region of the waveguides; in addition, the first hole in the Y-waveguide was displaced away from the cavity by $\delta S = 0.08a$.

Figures 1(b)–1(d) show the results of FDTD modeling, which illustrate how photon routing is achieved. The modeling was performed for a device with $r = 0.31a$ (73 nm). One should note that for our approach, it is essential that the fundamental modes in the H1 cavity are not degenerate. To lift the degeneracy in the model, an additional vertical displacement of two pairs of holes immediately above and below the cavity was introduced by $\delta a = 0.02a$ away from the cavity. Figure 1(b) presents the resulting cavity mode spectra, which were calculated from analysis of the decay transients of cavity fields using a method of harmonic inversion of time signals.[18] The unpolarised spectrum reveals two mode peaks split by 2.5 nm, consistent with experimental observations.

Notations X and Y, which are used for the W1 waveguides, reflect the orientation (at the cavity center) of the H_z dipole for a cavity mode, which is coupled to a respective waveguide. These modes are referred to as X- and Y-dipole modes.[19] Figures 1(c) and 1(d) show calculated H_z profiles for the non-degenerate X- and Y-dipole modes, respectively. The modes selectively couple to their corresponding waveguides. The polarised spectra in Fig. 1(b), calculated using *x*- and *y*-polarised dipole sources, demonstrate that the longer-wavelength (*x*-polarised) and shorter-wavelength (*y*-polarised) peaks correspond, respectively, to the Y- and X-dipole modes.

To quantify the strength of the cavity-waveguide coupling, Q-factors were calculated for each mode for an uncoupled cavity (i.e., with no waveguides), that with only a co-polarised waveguide and with only a cross-polarised waveguide present, Q_u, Q_{co}, and Q_{cross}, respectively. The Q-factors represent the loss rates in each case.[20] From that we found the loss rates into each waveguide and the strengths of co-coupling, $\eta_{co} = (Q_{co}^{-1} - Q_u^{-1})/Q_{tot}^{-1}$, and cross-coupling, $\eta_{cross} = (Q_{cross}^{-1} - Q_u^{-1})/Q_{tot}^{-1}$, where $Q_{tot} = (Q_{co}^{-1} + Q_{cross}^{-1} - Q_u^{-1})^{-1}$ is the Q-factor in case of both waveguides present. The calculated values of η_{co} and η_{cross} are, respectively, 89.5% and 2.1% for the X-dipole mode and 87.0% and 0.6% for the Y-dipole mode. The modeling results suggest that the co-coupling strength can be expected to significantly exceed cross-coupling in our structures.

Now we proceed to the experimental results. A schematic diagram of the sample, grown using molecular beam

epitaxy (MBE) on an undoped GaAs substrate, is shown in Fig. 2(a). A 200 nm thick *p-i-n* diode structure was grown on top of a 1 μm thick *n*-doped $Al_{0.6}Ga_{0.4}As$ sacrificial layer and a 1 μm thick *n*-doped GaAs contacting layer. A layer of nominally InAs SAQDs was grown in the middle of the diode using In-flush techniques[21,22] with a GaAs partial cap height of 2.5 nm and estimated density below $10^{10}\,cm^{-2}$. The dot layer was sandwiched between 5 nm GaAs spacer layers, 50 nm $Al_{0.3}Ga_{0.7}As$ barriers, and a 45 nm Si-doped *n*-type GaAs contact layer at the bottom and a Be-doped *p*-type GaAs contact layer at the top of the diode structure. The barriers were introduced to suppress tunnelling out of carriers in the electric field, enhancing the voltage tuning range over which SAQD emission could be observed.[23] The wafer was used to fabricate mesa diode devices of 400 μm diameter. Within each mesa, a number of suspended 200-nm thick PhC cavity membranes were fabricated using electron beam lithography and inductively coupled plasma etching, followed by etching away of the AlGaAs sacrificial layer in 40% HF. Each hexagonal PhC incorporated an H1 cavity and two W1 waveguides at 0° and 120°, which were terminated with Bragg outcouplers. An electron microscopy image of a typical PhC membrane is shown in Fig. 2(b).

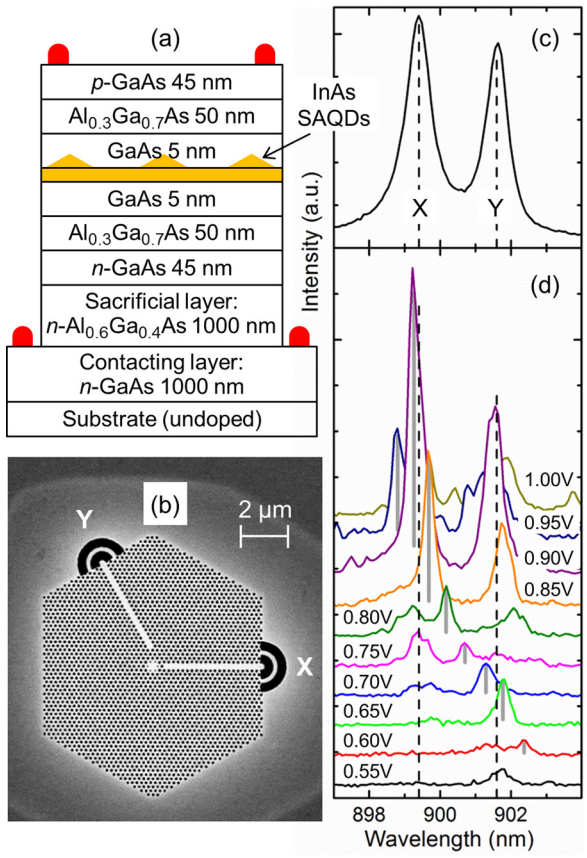

FIG. 2. (a) Schematic diagram of the sample wafer. The contacts are shown by red semi-circles. (b) An electron microscope image of a typical photonic crystal membrane with an H1 cavity. X and Y denote W1 waveguides terminating by Bragg outcouplers. (c) and (d) Photoluminescence spectra from the cavity. (c) Spectra at high excitation power of 35 μW and bias of 1.1 V. X and Y denote X- and Y-dipole modes. (d) Series of spectra at low excitation power of 1 μW at various biases. Spectra are offset for clarity. A single-dot peak which crosses both cavities is highlighted by grey vertical bars. Vertical dashed lines indicate wavelengths of the cavity mode maxima.

Micro-PL experiments with spatially resolved excitation and collection were performed in a continuous-flow liquid He cryostat at 5 K using a confocal-microscope setup. He-Ne laser excitation was provided to the cavity using a ×50 microscope objective and focused to a spot of 1–2 μm diameter. Emission was collected selectively either from the cavity or from one of the waveguide outcouplers, using the same objective and a single-mode optical fibre of 4.7 μm core diameter. The emission was dispersed by a 30 cm spectrometer and recorded using a liquid N_2 cooled CCD. Current-voltage characteristics at 5 K, typical for a *p-i-n* diode, showed clear rectifying behavior with the current onset at a forward bias of approximately 1.1 V. This value is slightly lower than expected for a planar GaAs diode; the reason for this is currently unclear, though it is in agreement with results reported in Ref. 15.

Under reverse bias (or at small forward bias), PL emission from the SAQD is typically not observed because the electric field causes photoexcited electrons and holes to tunnel out of the dot. At higher forward biases, however, tunneling out is suppressed, which leads to an increase of the SAQD PL emission. At high excitation power, ensemble dot emission is observed in reference spectra from unprocessed areas of the diodes. In the PhC structures, spectra collected from the cavities are dominated by cavity modes. In our sample, the typical splitting of the modes is 1–4 nm and the *Q*-factor is 1000–2000. Figure 2(c) shows a PL spectrum from one of the cavities at high excitation power. Two well pronounced cavity modes are observed at 899.3 nm and 901.7 nm. This PhC cavity has $r = 0.34a$ (80 nm), resulting in cavity modes that are blue shifted compared to the modelled spectra.

At low excitation power, exciton emission lines from individual SAQDs can be readily resolved in the cavity-collected spectra, as demonstrated in Fig. 2(d). With increasing voltage up to 1.1 V, the lines are blue shifted due to the QCSE. The typical range of the observed Stark shift is up to 5 nm, i.e., larger than the typical splitting of the cavity modes. It is worth noting that even when no individual dot emission lines are in resonance with the modes, the modes still dominate the cavity spectra at high excitation power due to cavity-feeding effects.[24–26]

Figure 2(d) shows a series of spectra from the same cavity as in Fig. 2(c) at low excitation power at various voltages. With voltage changing from 0.5 V to 1.0 V, a single-dot line (highlighted in the spectra) undergoes a blue shift from approximately 903 nm to 898 nm, crossing both modes. Figures 3(a) and 3(b) show, respectively, the dot line wavelength and intensity as a function of voltage at the same power; horizontal dashed lines indicate wavelengths of the cavity modes, while vertical dashed lines indicate the corresponding voltages, 0.67 V and 0.88 V, respectively, at which the dot line is in resonance with either mode. One can see that at both resonances, clear intensity peaks are observed. These are due to, first, Purcell enhancement of the spontaneous emission,[15,27] and second, preferential collection of the far-field emission from the cavity by the PL setup,[28] i.e., in both cases due to coupling of the dot emission to the cavity modes in the weak coupling regime. The intensity at the lower-voltage resonance (901.7 nm) is smaller, most likely because a significant fraction of photoexcited carriers tunnel

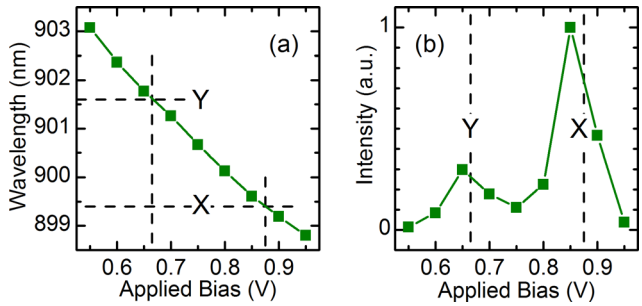

FIG. 3. Single-dot line wavelength (a) and intensity (b) as a function of bias in the spectra collected from the cavity. Solid lines are guides for the eye. Horizontal dashed lines indicate the wavelengths of the cavity X- and Y-mode maxima; vertical dashed lines indicate the voltages at which the dot line is observed at these wavelengths.

out of the dots at this voltage, while at the higher-voltage resonance (899.3 nm), tunneling out is suppressed.

In order to demonstrate routing, the outputs of the outcouplers were measured using the same low excitation power. Emission from the same single dot is observed in the spectra collected from both outcouplers, while laser excitation is provided to the cavity. To verify this, the line positions are followed as a function of voltage in the spectra collected both from the cavity and each of the outcouplers. These are presented in Fig. 4(a); it is clear that for the three collection geometries, the line positions coincide.

Figure 4(b) shows the intensity of the same QD line as a function of voltage for collection from the X and Y outcouplers. Results for cavity collection from Fig. 3(b) are also presented for comparison; the plots are normalized to their respective maximum values. (In absolute terms, the maximum emission intensity for the X outcoupler is approximately 5 times larger than for the Y outcoupler and is 10% of that for cavity collection.) One can see that for collection from the X outcoupler, the line intensity peaks at the resonance with the X-mode at 899.3 nm. On the contrary, in the spectra collected from the Y outcoupler, the maximum intensity is observed at the resonance with the Y-mode at 901.7 nm, while at the resonance with the X-mode, the line almost vanishes, even though it is at its maximum value in the spectra collected from the cavity. Comparison of absolute values of intensities provides estimates of branching ratios (i.e., ratios of co-coupling to cross-coupling) at resonances

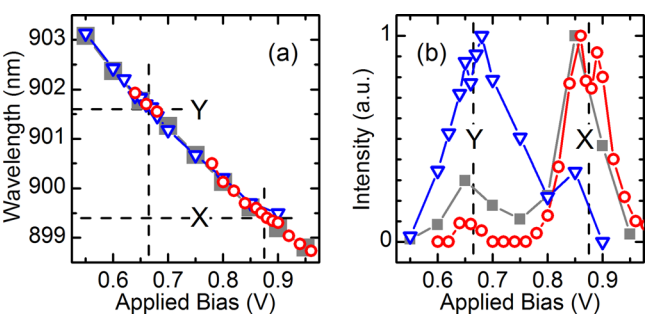

FIG. 4. Single-dot line wavelength (a) and intensity (b) as a function of bias in the spectra collected from the cavity, X and Y outcouplers (grey squares, red circles, and blue triangles, respectively). Line intensities are normalized. The meaning of the dashed lines is the same as in Fig. 3.

with both modes. We obtain a good branching ratio of 12:1 for the resonance with the X-mode and a moderate ratio of 3:1 for that with the Y-mode. Clearly, these ratios are significantly lower than predicted by theoretical calculations. This is most likely due to fabrication imperfections of PhC membrane structures. Fabry-Perot modes in the waveguides may also contribute.

These observations unambiguously demonstrate electrically controlled selective routing of the single-dot emission to the waveguides. They provide convincing evidence that the mechanism of routing is based on a combination of two types of coupling: first, resonant coupling of single-dot emission to the cavity modes, which is tunable by means of the QCSE, and second, preferential coupling of the cavity modes to the respective waveguides, which is achieved by the PhC cavity design.

To conclude, we have demonstrated that photonic crystal nanocavities with incorporated waveguides can be employed for voltage-controlled selective routing of emission from single quantum dots. This proof of concept provides the basis for scalable, low-power, high-speed operation of on-chip single-photon routers for use in integrated quantum photonic circuits.

This work was funded by EPSRC Grant No. EP/J007544/1.

[1]J. L. O'Brien, A. Furusawa, and J. Vuckovic, Nat. Photonics **3**, 687 (2009).
[2]P. Lodahl, S. Mahmoodian, and S. Stobbe, Rev. Mod. Phys. **87**, 347 (2014).
[3]A. J. Shields, Nat. Photonics **1**, 215 (2007).
[4]Y.-M. He, Y. He, Y.-J. Wei, D. Wu, M. Atatuere, C. Schneider, S. Hoefling, M. Kamp, C.-Y. Lu, and J.-W. Pan, Nat. Nanotechnol. **8**, 213 (2013).
[5]A. Faraon, I. Fushman, D. Englund, N. Stoltz, P. Petroff, and J. Vuckovic, Nat. Phys. **4**, 859 (2008).
[6]D. Tiarks, S. Baur, K. Schneider, S. Duerr, and G. Rempe, Phys. Rev. Lett. **113**, 053602 (2014).
[7]M. A. Pooley, D. J. P. Ellis, R. B. Patel, A. J. Bennett, K. H. A. Chan, I. Farrer, D. A. Ritchie, and A. J. Shields, Appl. Phys. Lett. **100**, 211103 (2012).
[8]D. Englund, A. Faraon, B. Y. Zhang, Y. Yamamoto, and J. Vuckovic, Opt. Express **15**, 5550 (2007).
[9]A. Schwagmann, S. Kalliakos, I. Farrer, J. P. Griffiths, G. A. C. Jones, D. A. Ritchie, and A. J. Shields, Appl. Phys. Lett. **99**, 261108 (2011).
[10]A. Laucht, S. Pütz, T. Günthner, N. Hauke, R. Saive, S. Frédérick, M. Bichler, M.-C. Amann, A. W. Holleitner, M. Kaniber, and J. J. Finley, Phys. Rev. X **2**, 011014 (2012).
[11]R. J. Coles, N. Prtljaga, B. Royall, I. J. Luxmoore, A. M. Fox, and M. S. Skolnick, Opt. Express **22**, 2376 (2014).
[12]S. Mosor, J. Hendrickson, B. C. Richards, J. Sweet, G. Khitrova, H. M. Gibbs, T. Yoshie, A. Scherer, O. B. Shchekin, and D. G. Deppe, Appl. Phys. Lett. **87**, 141105 (2005).
[13]A. Kiraz, P. Michler, C. Becher, B. Gayral, A. Imamoglu, L. D. Zhang, E. Hu, W. V. Schoenfeld, and P. M. Petroff, Appl. Phys. Lett. **78**, 3932 (2001).
[14]P. W. Fry, I. E. Itskevich, D. J. Mowbray, M. S. Skolnick, J. J. Finley, J. A. Barker, E. P. O'Reilly, L. R. Wilson, I. A. Larkin, P. A. Maksym, M. Hopkinson, M. Al-Khafaji, J. P. R. David, A. G. Cullis, G. Hill, and J. C. Clark, Phys. Rev. Lett. **84**, 733 (2000).
[15]A. Laucht, F. Hofbauer, N. Hauke, J. Angele, S. Stobbe, M. Kaniber, G. Bohm, P. Lodahl, M. C. Amann, and J. J. Finley, New J. Phys. **11**, 023034 (2009).
[16]A. F. Oskooi, D. Roundy, M. Ibanescu, P. Bermel, J. D. Joannopoulos, and S. G. Johnson, Comput. Phys. Commun. **181**, 687 (2010).
[17]M. Shirane, S. Kono, J. Ushida, S. Ohkouchi, N. Ikeda, Y. Sugimoto, and A. Tomita, J. Appl. Phys. **101**, 073107 (2007).

[18]V. A. Mandelshtam and H. S. Taylor, J. Chem. Phys. **107**, 6756 (1997).
[19]The notations *do not* reflect the direction of the electric field in a dipole cavity mode; on the contrary, the predominant orientation of the electric field in the X-dipole mode is along the *y* coordinate axis, and vice versa.
[20]A. Faraon, E. Waks, D. Englund, I. Fushman, and J. Vuckovic, Appl. Phys. Lett. **90**, 073102 (2007).
[21]Z. R. Wasilewski, S. Fafard, and J. P. McCaffrey, J. Cryst. Growth **201**, 1131 (1999).
[22]S. Fafard, Z. R. Wasilewski, C. N. Allen, D. Picard, M. Spanner, J. P. McCaffrey, and P. G. Piva, Phys. Rev. B **59**, 15368 (1999).
[23]A. J. Bennett, R. B. Patel, J. Skiba-Szymanska, C. A. Nicoll, I. Farrer, D. A. Ritchie, and A. J. Shields, Appl. Phys. Lett. **97**, 031104 (2010).
[24]A. Badolato, M. Winger, K. J. Hennessy, E. L. Hu, and A. Imamoglu, C. R. Phys. **9**, 850 (2008).
[25]M. Kaniber, A. Laucht, A. Neumann, J. M. Villas-Boas, M. Bichler, M. C. Amann, and J. J. Finley, Phys. Rev. B **77**, 161303 (2008).
[26]M. Winger, T. Volz, G. Tarel, S. Portolan, A. Badolato, K. J. Hennessy, E. L. Hu, A. Beveratos, J. Finley, V. Savona, and A. Imamoglu, Phys. Rev. Lett. **103**, 207403 (2009).
[27]E. M. Purcell, Phys. Rev. **69**, 681 (1946).
[28]B. Gayral and J. M. Gerard, Phys. Rev. B **78**, 235306 (2008).